Modeling Cross-Modal Enhancement and Modality-Specific Suppression in Multisensory Neurons

Paul E. Patton
ppatton@uiuc.edu
Beckman Institute, University of Illinois at Urbana/Champaign,
Urbana, IL 61801, U.S.A.

Thomas J. Anastasio
tja@uiuc.edu
Beckman Institute and Department of Molecular and Integrative Physiology,
University of Illinois at Urbana/Champaign, Urbana, IL 61801, U.S.A.

Cross-modal enhancement (CME) occurs when the neural response to a stimulus of one modality is augmented by another stimulus of a different modality. Paired stimuli of the same modality never produce supra-additive enhancement but may produce modality-specific suppression (MSS), in which the response to a stimulus of one modality is diminished by another stimulus of the same modality. Both CME and MSS have been described for neurons in the deep layers of the superior colliculus (DSC), but their neural mechanisms remain unknown. Previous investigators have suggested that CME involves a multiplicative amplifier, perhaps mediated by N-methyl D-aspartate (NMDA) receptors, which is engaged by cross-modal but not modality-specific input. We previously postulated that DSC neurons use multisensory input to compute the posterior probability of a target using Bayes' rule. The Bayes' rule model reproduces the major features of CME. Here we use simple neural implementations of our model to simulate both CME and MSS and to argue that multiplicative processes are not needed for CME, but may be needed to represent input variance and covariance. Producing CME requires only weighted summation of inputs and the threshold and saturation properties of simple models of biological neurons. Multiplicative nodes allow accurate computation of posterior target probabilities when the spontaneous and driven inputs have unequal variances and covariances. Neural implementations of the Bayes' rule model account better than the multiplicative amplifier hypothesis for the effects of pharmacological blockade of NMDA receptors on the multisensory responses of DSC neurons. The neural implementations also account for MSS, given only the added hypothesis that input channels of the same modality have more spontaneous covariance than those of different modalities.

1 Introduction

Multisensory integration occurs at numerous sites in the mammalian nervous system (Stein & Meredith, 1993) and has been studied extensively in the deep layers of the superior colliculus (DSC) of cats and monkeys (Meredith & Stein, 1986b; Wallace, Wilkinson, & Stein, 1996; Wallace, Meredith, & Stein, 1998). Enhancement is a form of multisensory integration in which the response to a stimulus of one modality is augmented by a stimulus of another modality (Meredith & Stein, 1986b; Stein & Meredith, 1993). Cross-modal enhancement (CME) was thought to be mediated by multiplicative interactions among inputs of different modalities, perhaps through N-methyl D-aspartate (NMDA) receptors present in DSC neurons (Meredith & Stein, 1986b; Stein, Huneycutt, & Meredith, 1988; Meredith, Wallace, & Stein, 1992; Stein & Meredith, 1993; Binns & Salt, 1996; Binns, 1999). CME contrasts sharply with the responses of multisensory neurons to paired stimuli of the same modality presented within their excitatory receptive fields. Such presentations never produce robust enhancement of the sort seen in CME and sometimes result in modality-specific suppression (MSS), in which the response to a stimulus of one modality is reduced by a second stimulus of the same modality (Stein & Meredith, 1993). The neural mechanisms of CME and MSS remain unknown. Open questions concern whether CME requires multiplicative interactions, the possible role of NMDA receptors, and the paradox of MSS. In previous work we modeled CME on an abstract level using Bayes' rule (Anastasio, Patton, & Belkacem-Boussaid, 2000). Here we use neural implementations of the Bayes' rule model to explore mechanisms of multisensory integration in DSC and other neurons.

The DSC receives visual, auditory, and somatosensory inputs organized as a multimodal topographic map (Middlebrooks & Knudsen, 1984; Meredith & Stein, 1990; Clemo & Stein, 1991). Activation of cells at a particular location in this map can result in an orienting movement toward the corresponding location in space containing the stimulus source (Wurtz & Goldberg, 1972; Peck, 1990). Individual DSC neurons may receive input from two, or occasionally three, different sensory modalities (Meredith et al., 1992; Wallace et al., 1996). Receptive fields for multiple modalities are large and spatially coincident. CME in multisensory DSC neurons occurs when stimuli of different modalities are presented together within their excitatory receptive fields (Meredith & Stein, 1996; Kadunce, Vaughan, Wallace, & Stein, 2001). Enhancement can be expressed as a percentage of the largest single stimulus response SR_{max},

$$\%E = \frac{CR - SR_{max}}{SR_{max}} \times 100\%, \tag{1.1}$$

where CR is the neural response to the combined stimuli. CME exhibits the property of inverse effectiveness, wherein weak unimodal stimuli, when

combined, produce a larger %*E* than do stronger stimuli (Meredith & Stein, 1986b; Wallace & Stein, 1994; Wallace et al., 1996). Multimodal neurons exhibiting CME have also been described in cat extraprimary sensory cortex (Wallace, Meredith, & Stein, 1992; Jiang, Lepore, Ptito, & Guillemot, 1994; Stein & Wallace, 1996), and cross-modal enhancement phenomena have been noted in the behavioral responses of cats (Stein et al., 1988; Stein, Meredith, Huneycutt, & McDade, 1989). MSS observed for DSC neurons can be expressed as negative percentage enhancement. Modality-specific suppressive interactions have also been reported for neurons in a number of primate cortical visual structures (Sato, 1989, 1995; Reynolds, Chelazzi, & Desimone, 1999).

We have proposed previously that DSC neurons use stochastic sensory input to compute the posterior probability of a target using Bayes' rule (Anastasio et al., 2000). We showed that CME and inverse effectiveness arise as straightforward consequences of this hypothesis. The initial study did not address the issue of how neurons might implement the needed computation. That posterior probabilities are a natural outcome of neural computation is well known to specialists in neural networks and pattern classification (Richard & Lippmann, 1991; Duda, Hart, & Stork, 2001). We apply these results in a neurobiological context and extend them to account for experimental observations.

To illustrate how the Bayes' rule model of CME (Anastasio et al., 2000) might be implemented by neurons, we consider three simple perceptron models. The simplest involves a single perceptron with sensory input channels that are Poisson distributed and conditionally independent. This model demonstrates that enhancement can be produced using only properties generically present in biological neurons and that no special multiplicative interactions are needed. The second, an augmented perceptron model, computes posterior probabilities under the more general circumstances in which inputs are multivariate gaussian. We show that it accounts better than the multiplicative interaction hypothesis for experimental findings on the effects of NMDA receptor blockade on the responses of DSC neurons. The third implementation extends the Bayes' rule model to provide an explanation for the otherwise puzzling phenomenon of MSS. The augmented perceptron produces suppression given neurobiologically plausible assumptions that include covariance among inputs of like modality in the absence of sensory stimulation.

2 A Perceptron Model with Poisson Inputs Can Simulate CME

We first consider a model in which the sensory input likelihoods are Poisson distributed and conditionally independent given the target. Under these conditions, a single perceptron is capable of computing the posterior probability of a target and simulating CME. The target is represented as binary random variable T (target absent, $T = 0$; target present, $T = 1$). The prior

probability distribution of the target is assigned arbitrarily as $P(T = 1) = 0.1$ and $P(T = 0) = 0.9$. According to the Bayes' rule model (Anastasio et al., 2000), the posterior probability of a target is computed by using sensory input to modify this prior probability. Input from each modality i is modeled as random variable $M_i(i = 1, 2, \ldots, k)$, which can assume any discrete non-negative value m_i. The m_i represent numbers of neural impulses per unit time (firing rate). The input likelihoods, which are conditional distributions of the inputs given the target, are modeled as Poisson densities:

$$P(M_i = m_i \mid T = t) = \frac{\lambda_{it}^{m_i} e^{-\lambda_{it}}}{m_i!}. \tag{2.1}$$

The Poisson density was used in the original formulation of the Bayes' rule model (Anastasio et al., 2000) because it requires the fewest assumptions and reasonably approximates neuronal firing-rate distributions (Gabbiani & Koch, 1998). The mean and variance of a Poisson distribution are equal and are specified by parameter λ. The input likelihoods under spontaneous (target absent, $P(M_i = m_i \mid T = 0)$) or driven (target present, $P(M_i = m_i \mid T = 1)$) conditions are described using equation 2.1 with means λ_{i0} and λ_{i1}, respectively ($\lambda_{i1} > \lambda_{i0}$) (see Figure 1B). The posterior target probability is

Figure 1: *Facing page.* (A) A perceptron model of multisensory integration. The model receives two conditionally independent Poisson-distributed sensory inputs, $M_1 = V$ and $M_2 = A$, having synaptic weights w_v and w_a. The bias input b is fixed and might represent tonic inhibitory input or biophysical properties intrinsic to a neuron. The sigma node Σ computes the weighted sum u of the inputs (see equation 2.5). The output is passed through the logistic squashing function $f(u)$ (see equation 2.6). (B) The likelihoods of observing discrete numbers of impulses per unit time (0.25 s) are shown for sensory input M_i under spontaneous ($P(M_i = m_i \mid T = 0)$, spont, dot-dashed line) and stimulus driven ($P(M_i = m_i \mid T = 1)$, driven, solid line) conditions. The likelihoods are given by Poisson distributions (see equation 2.1) with $\lambda_{i0} = 2$ and $\lambda_{i1} = 6$. (C) The bimodal perceptron model simulates CME. The response is equal to the posterior probability of a target as computed by the perceptron ($f(u) = P(T = 1 \mid \mathbf{m})$) using equations 2.5, 2.6, and 2.8. For both modalities V and A, the input likelihoods are assigned spontaneous mean $\lambda_{v0} = \lambda_{a0} = 2$ and driven mean $\lambda_{v1} = \lambda_{a1} = 6$. In the cross-modal both-driven case (stars), both modalities are driven by a target stimulus. Inputs $V = v$ and $A = a$ are set equal and varied over a range of impulses per unit time. In the modality-specific spontaneous-driven case (circles), one modality is driven, while the other is fixed at the spontaneous mean. The difference between the two plots represents CME. The dashed line indicates prior target probability $P(T = 1)$. The both-driven and spontaneous-driven plots represent slices through the full 2D posterior. (D) Cross-modal enhancement for the perceptron model is computed using equation 1.1, where CR and SR_{max} values are taken from the both-driven and spontaneous-driven curves of C.
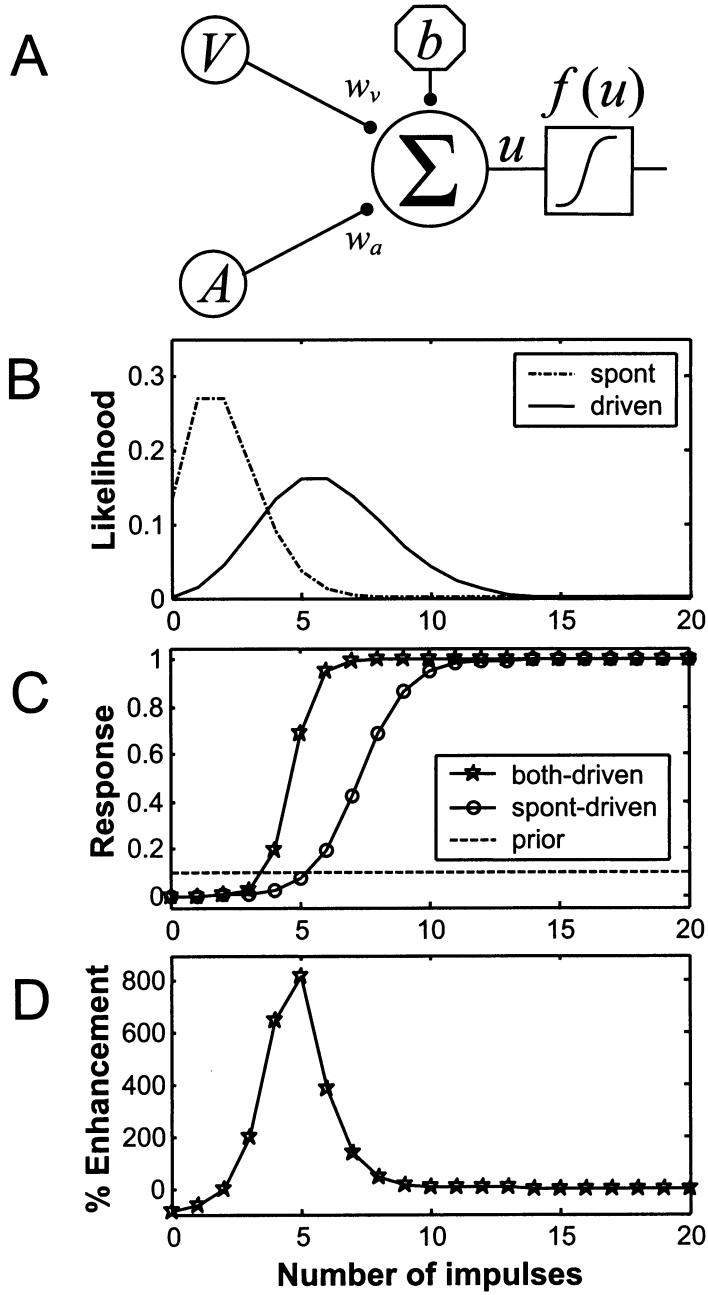
given using Bayes' rule:

$$P(T = 1 \mid \mathbf{m}) = \frac{P(\mathbf{m} \mid T = 1)P(T = 1)}{P(\mathbf{m})}. \tag{2.2}$$

In this equation, $\mathbf{m}$ is a vector representing the activity m_i of each sensory modality M_i. We assume initially that the likelihoods for the various modalities are conditionally independent given the target. According to this simplifying assumption, the visibility of a target indicates nothing about its audibility, and vice versa. The joint likelihoods $P(\mathbf{m} \mid T = 1)$ and $P(\mathbf{m} \mid T = 0)$ can then be computed as

$$P(\mathbf{m} \mid T = t) = \prod_{i=1}^{k} P(M_i = m_i \mid T = t). \tag{2.3}$$

The unconditional joint probability $P(\mathbf{m})$ is given by the principle of total probability:

$$P(\mathbf{m}) = P(T = 1)P(\mathbf{m} \mid T = 1) + P(T = 0)P(\mathbf{m} \mid T = 0). \tag{2.4}$$

We will use the perceptron as the basis for our model of a DSC neuron. The perceptron computes the weighted sum u of its inputs where each input m_i has an associated synaptic weight w_i:

$$u = b + \sum_{i=1}^{k} w_i m_i. \tag{2.5}$$

The constant bias input b might represent the biophysical properties of a neuron or a tonic input. The weighted input sum is passed through the logistic squashing function,

$$f(u) = \frac{1}{1 + e^{-u}}, \tag{2.6}$$

which approximates the threshold and saturation properties of real neurons.

We seek a formula for u such that the value of the logistic function $f(u)$ is equal to the posterior probability of the target given inputs $\mathbf{m}(f(u) = P(T = 1 \mid \mathbf{m}))$. We substitute equation 2.6 for $f(u)$ and substitute Poisson distributions 2.1 for the input likelihoods in equations 2.2, 2.3, and 2.4. In solving for u, we obtain:

$$u = ln\left[\frac{P(T = 1)}{P(T = 0)}\right] + \sum_{i=1}^{k}\left[\left(ln\left(\frac{\lambda_{i1}}{\lambda_{i0}}\right)\right)m_i + (\lambda_{i0} - \lambda_{i1})\right]. \tag{2.7}$$

Equation 2.7 is linear with respect to m_i. Thus, given the basic neuronal nonlinearities of threshold and saturation as represented by the squashing function, the posterior probability is computed by the weighted sum of sensory inputs. Multiplying inputs together is not necessary. This finding contrasts with previous ideas about the neural basis of CME (see section 5). Equation 2.7 can be rearranged to yield the input weights w_i and bias b for a simple perceptron (see Figure 1A):

$$w_i = ln\left(\frac{\lambda_{i1}}{\lambda_{i0}}\right) \text{ and } b = ln\left[\frac{P(T=1)}{P(T=0)}\right] + \sum_{i=1}^{k}(\lambda_{i0} - \lambda_{i1}). \tag{2.8}$$

The bias contains a term related to the target prior. Because $\lambda_{i1} > \lambda_{i0}$, the bias term will be negative whenever $P(T = 1) < P(T = 0)$. This finding has interesting implications for how the target prior might be represented neurobiologically (see section 5).

We propose that the response of a DSC neuron is proportional to posterior target probability. A perceptron with weights set according to equation 2.8 was used to simulate the results of a bimodal CME experiment. We consider visual V and auditory A inputs, but the simulation is valid for any combination of two sensory modalities. To simulate the response of a bimodal DSC neuron to cross-modal stimulation, modalities $M_1 = V$ and $M_2 = A$ were set equal and varied from 0 to 25 impulses per unit time (both-driven). To simulate a bimodal DSC neuron's response to modality-specific stimulation, one input was varied from 0 to 25 impulses per unit time, while the other was held fixed at its spontaneous mean (spontaneous-driven). The results are illustrated in Figures 1C and 1D. A single perceptron is thus sufficient to implement the Bayes' rule model of CME for inputs that are Poisson distributed and conditionally independent given the target.

3 An Augmented Perceptron Model and the Role of NMDA Receptors

As a more general form of our model, we consider a case in which sensory inputs are represented as gaussian distributions, and we drop the assumption that inputs from different modalities are conditionally independent given the target. Input to a DSC neuron from a single sensory modality is derived by combining signals from many different sensory neurons. According to the classical central limit theorem, the distribution of the combined input will be gaussian, provided that the individual signals are independent (Fristedt & Gray, 1997). We assume that input from a single modality will be approximately gaussian, despite possible dependencies between signals carried by individual neurons of the same modality (see below). We model the multimodal input and dependencies between inputs of different

modalities using a multivariate gaussian distribution (Duda et al., 2001):

$$P(\mathbf{m} \mid T=t) = \frac{1}{(2\pi)^{k/2}|\boldsymbol{\Sigma}_t|^{1/2}} \exp\left[-\frac{1}{2}(\mathbf{m}-\boldsymbol{\mu}_t)^{\mathrm{T}}\boldsymbol{\Sigma}_t^{-1}(\mathbf{m}-\boldsymbol{\mu}_t)\right]. \quad (3.1)$$

In this equation, k is the number of modalities, and $\boldsymbol{\mu}_t$ is a vector containing the means of the distributions associated with each modality when $T = t$. The symbol T denotes the transpose operation. $\boldsymbol{\Sigma}_t$ is a k by k covariance matrix whose diagonal terms are the variances associated with individual modalities and whose off-diagonal terms are the covariances among modalities.

The model classifies input patterns into two categories: $T = 0$ and $T = 1$. For this simple case, u can be expressed as a discriminant function (Duda et al., 2001):

$$u = g(\mathbf{m}) = \ln\left(\frac{P(T=1 \mid \mathbf{m})}{P(T=0 \mid \mathbf{m})}\right) = \ln\left(\frac{P(\mathbf{m} \mid T=1)}{P(\mathbf{m} \mid T=0)}\right) + \ln\left(\frac{P(T=1)}{P(T=0)}\right)$$

$$= \ln P(\mathbf{m} \mid T=1) + \ln P(T=1) - [\ln P(\mathbf{m} \mid T=0) + \ln P(T=0)]. \quad (3.2)$$

Substituting equation 3.1 and simplifying, we obtain:

$$u = \frac{1}{2}[\mathbf{m}^{\mathrm{T}}(\boldsymbol{\Sigma}_1^{-1} - \boldsymbol{\Sigma}_0^{-1})\mathbf{m} + 2\mathbf{m}^{\mathrm{T}}(\boldsymbol{\Sigma}_1^{-1}\boldsymbol{\mu}_1 - \boldsymbol{\Sigma}_0^{-1}\boldsymbol{\mu}_0)$$

$$- \boldsymbol{\mu}_1^{\mathrm{T}}\boldsymbol{\Sigma}_1^{-1}\boldsymbol{\mu}_1 + \boldsymbol{\mu}_0^{\mathrm{T}}\boldsymbol{\Sigma}_0^{-1}\boldsymbol{\mu}_0]$$

$$+ \ln\left(\frac{|\boldsymbol{\Sigma}_0|^{1/2}P(T=1)}{|\boldsymbol{\Sigma}_1|^{1/2}P(T=0)}\right). \quad (3.3)$$

As before, the subscript 1 refers to an input driven by the target stimulus ($T = 1$), and 0 to one active spontaneously in the absence of a stimulus ($T = 0$). Because of the quadratic and multiplicative terms involved, this formula cannot, in general, be implemented by a single perceptron.

A multilayered perceptron is capable of approximating any continuous function (Cybenko, 1989). Such a network, given **m** as input and appropriate synaptic weights, should be capable of supplying an approximation of u in equation 3.3 to a logistic output node representing a DSC neuron. Another plausible implementation involves the introduction of pi nodes, or product units (Rumelhart, Hinton, & McClelland, 1986; Durbin & Rumelhart, 1989), to create an augmented-perceptron model (see Figure 2A). Pi nodes multiply their inputs together just as sigma nodes add them. Neurobiologically, they represent possible voltage-sensitive processes in the dendritic arbor of a neuron (Durbin & Rumelhart, 1989; Koch & Poggio, 1992). The augmented-perceptron model can be expressed as

$$u = b + \sum_{i=1}^{k} w_i m_i + \sum_{i=1}^{k} \sum_{j=i}^{k} \rho_{ij}(m_i m_j). \quad (3.4)$$

The first two terms on the right-hand side are identical with those of the simple perceptron, equation 2.5. The last term specifies the sigma-pi function with weights ρ_{ij}. For the case of two sensory inputs $V = v$ and $A = a$, equation 3.4 can be rewritten as

$$u = b + w_v v + w_a a + \rho_v v^2 + \rho_a a^2 + \rho_{va} va. \tag{3.5}$$

Using equation 3.3, the constants ρ_v, ρ_a, ρ_{va}, w_v, w_a, and b can be specified as

$$\rho_v = \frac{1}{2}\left(\frac{\sigma_{a0}^2}{\beta_0} - \frac{\sigma_{a1}^2}{\beta_1}\right), \; \rho_a = \frac{1}{2}\left(\frac{\sigma_{v0}^2}{\beta_0} - \frac{\sigma_{v1}^2}{\beta_1}\right), \; \rho_{va} = \left(\frac{\sigma_{va1}^2}{\beta_1} - \frac{\sigma_{va0}^2}{\beta_0}\right), \tag{3.6}$$

$$w_v = \left(\frac{\mu_{v1}\sigma_{a1}^2 - \mu_{a1}\sigma_{va1}^2}{\beta_1}\right) + \left(\frac{\mu_{a0}\sigma_{va0}^2 - \mu_{v0}\sigma_{a1}^2}{\beta_0}\right), \tag{3.7}$$

$$w_a = \left(\frac{\mu_{a1}\sigma_{v1}^2 - \mu_{v1}\sigma_{va1}^2}{\beta_1}\right) + \left(\frac{\mu_{v0}\sigma_{va0}^2 - \mu_{a0}\sigma_{v1}^2}{\beta_0}\right), \tag{3.8}$$

$$b = \frac{[-\sigma_{a1}^2\mu_{v1}^2 + 2\sigma_{va1}^2\mu_{v1}\mu_{a1} - \sigma_{v1}^2\mu_{a1}^2]}{2\beta_1}$$

$$+ \frac{[\sigma_{a0}^2\mu_{v0}^2 - 2\sigma_{va0}^2\mu_{v0}\mu_{a0} + \sigma_{v0}^2\mu_{a0}^2]}{2\beta_0}$$

$$+ \ln\left[\left(\sqrt{\frac{\beta_0}{\beta_1}}\right)\frac{P(T=1)}{P(T=0)}\right]. \tag{3.9}$$

In these equations, $\beta_0 = \sigma_{v0}^2\sigma_{a0}^2 - \sigma_{vao}^4$ and $\beta_1 = \sigma_{v1}^2\sigma_{a1}^2 - \sigma_{va1}^4$. The terms $\sigma_{v0}^2, \sigma_{a0}^2, \sigma_{v1}^2$, and σ_{a1}^2 are variances for the spontaneous and driven cases for each modality, and σ_{va0}^2 and σ_{va1}^2 are the covariances for the spontaneous and driven conditions, respectively.

An augmented perceptron as specified by equations 3.5 through 3.9 can compute posterior target probability and thereby simulate CME (see Figures 2B and 2C). Note that as for the Poisson-input model, CME arises by summation in a nonlinear neuron. When the spontaneous and driven variances and the spontaneous and driven covariances are equal ($\sigma_{v0}^2 = \sigma_{v1}^2, \sigma_{a0}^2 = \sigma_{a1}^2$, and $\sigma_{va0}^2 = \sigma_{va1}^2$), the pi-node terms disappear ($\rho_v = \rho_a = \rho_{va} = 0$) and the computation can again be performed by a simple perceptron. The multiplicative terms associated with the pi nodes compensate for differences between spontaneous and driven variance and covariance rather than produce CME.

Targets vary greatly in the efficacy with which they drive different sensory input neurons. It seems likely that the variance of a sensory input of any modality should be larger in the driven than in the spontaneous case.
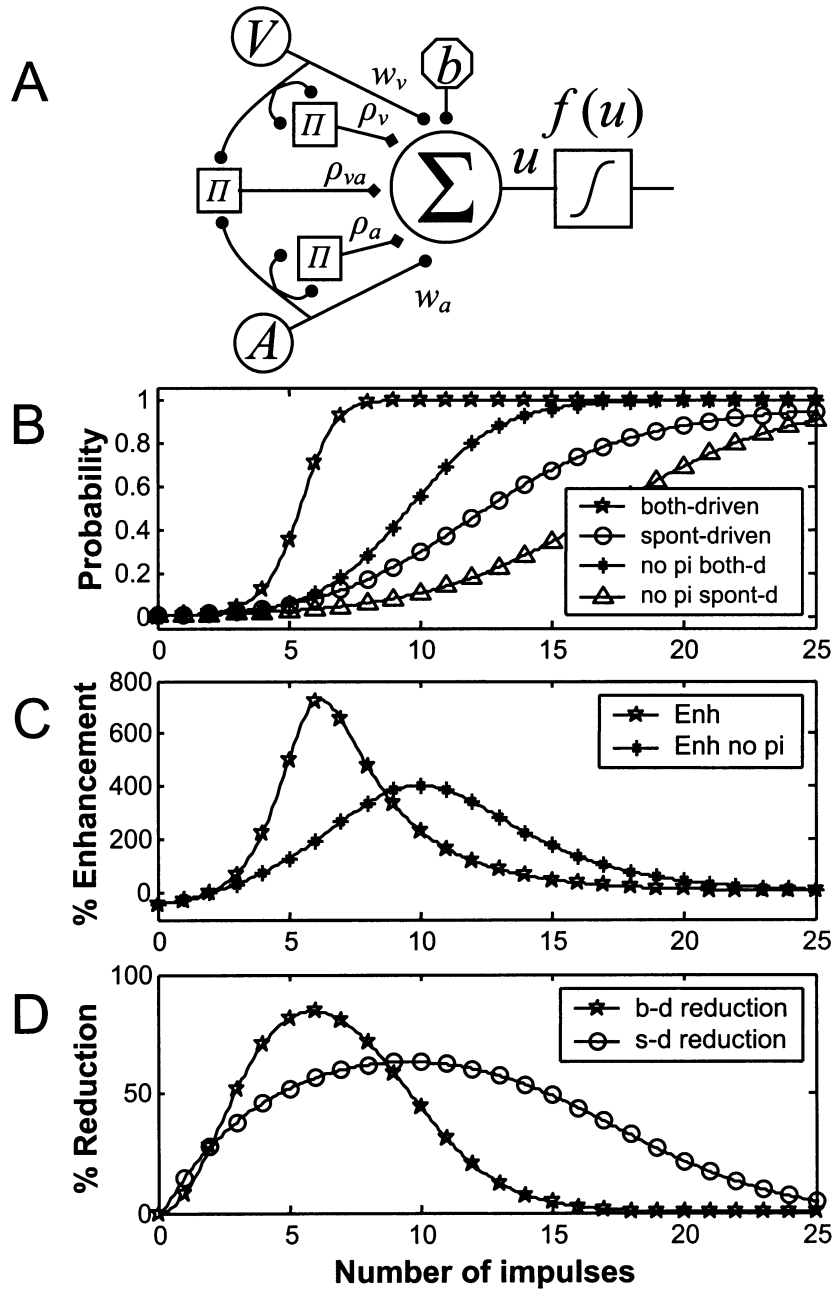
In the two-channel model, we set the spontaneous variances $\sigma_{v0}^2 = \sigma_{a0}^2 = 5$ and the driven variances $\sigma_{v1}^2 = \sigma_{a1}^2 = 6$. It also seems likely that two sensory inputs of different modalities should covary more under driven than under spontaneous conditions. Inputs of different modalities are segregated in modality-specific pathways prior to their arrival in the DSC (Sparks & Hartwich-Young, 1989; Wallace, Meredith, & Stein, 1993). Such input channels are unlikely to interact under spontaneous conditions, and sponta-

---

Figure 2: *Facing page*. (A) An augmented-perceptron model of multisensory integration. Sensory inputs are gaussian distributed. The model receives input from two sensory modalities: $M_1 = V$ and $M_2 = A$. Each provides weighted input to summing node Σ with weights w_v and w_a. The summing node also receives a fixed bias input b. The set of three pi nodes Π multiplies both modalities by themselves and by each other. The pi nodes provide inputs to the summing node with weights ρ_v, ρ_a, and ρ_{va}. The output is passed through the squashing function $f(u)$. (B) The augmented-perceptron model simulates CME. Input likelihoods are gaussian distributed. For both modalities V and A, the spontaneous likelihood mean is $\mu_{v0} = \mu_{a0} = 2$, and the driven likelihood mean is $\mu_{v1} = \mu_{a1} = 6$. Spontaneous and driven variances for both modalities are $\sigma_{v0}^2 = \sigma_{a0}^2 = 5$ and $\sigma_{v1}^2 = \sigma_{a1}^2 = 6$. The spontaneous and driven covariances are $\sigma_{va0}^2 = 0.1$ and $\sigma_{va1}^2 = 2.8$. The responses are equal to posterior target probability computed using the augmented perceptron. The cross-modal both-driven curve (stars) simulates a case in which both modalities are driven by a stimulus. Inputs $V = v$ and $A = a$ are set equal and varied from 0 to 25 impulses per unit time. The modality-specific spontaneous-driven curve (circles) simulates a case where only one modality is driven. The driven input varies from 0 to 25 impulses per unit time, while the input representing the nondriven modality was held fixed at the mean of the spontaneous likelihood distribution. The both-driven and spontaneous-driven plots represent slices through the full 2D posterior. The no pi both-driven (asterisks) and no pi spontaneous-driven (triangles) curves illustrate the inaccurate probability computation performed for the both-driven and spontaneous-driven cases, respectively, by a network in which the pi nodes have been removed by setting $\rho_v = \rho_a = \rho_{va} = 0$. (C) Cross-modal enhancement (see equation 1.1) is plotted for the intact augmented perceptron (stars) and for a version from which the pi nodes have been removed (asterisks). (D) The amount by which removal of the pi nodes reduces the augmented perceptron response to input is illustrated for the both-driven (asterisks) and spontaneous-driven (circles) cases. In each case, reduction R is computed using

$$R = \frac{P(T = 1 \mid \mathbf{m}) - L(\mathbf{m})}{P(T = 1 \mid \mathbf{m})} \times 100\%,$$

where $P(T = 1 \mid \mathbf{m})$ is computed using the intact network, and $L(\mathbf{m})$ is the corresponding value computed by the lesioned network following removal of the pi nodes.

neous covariance between channels of different modalities should be low. In contrast, the sensory attributes of natural targets are likely to covary, and channels of different modalities will covary as they are driven by these targets. Accordingly, in the two-channel model, we set spontaneous covariance $\sigma_{va0}^2 = 0.1$ and driven covariance $\sigma_{va1}^2 = 2.8$.

The specific variance and covariance values chosen are consistent with these plausible assumptions and produce an accurate simulation of neurophysiological findings on DSC neurons when used to parameterize the two-channel augmented perceptron. An augmented-perceptron model DSC neuron receiving inputs of two modalities (see Figure 2A) is studied in the both-driven case, in which both modalities are driven equally by a stimulus, and in the spontaneous- driven case, in which one modality is driven by a stimulus while the other is spontaneously active. As the number of impulses increases, target probability increases from nearly zero to nearly one, and it increases faster in the both-driven than in the spontaneous-driven case (see Figure 2B). CME reaches its highest values in the region where the spontaneous-driven responses are still small (see Figures 2B and 2C). Presumably, experimental effects on CME would be studied in this region, which will be referred to as the enhancement zone.

Binns and Salt (1996) investigated the effects of pharmacologically blocking NMDA receptors on the responses of DSC neurons to modality-specific and cross-modal stimuli. We postulate that NMDA receptors may serve the functional role assigned to pi nodes in the augmented-perceptron model. To investigate this hypothesis, the effects on the model of removing the pi nodes (i.e., setting $\rho_v = \rho_a = \rho_{va} = 0$) were compared with the effects reported by Binns and Salt (1996). Following pi node removal, the model no longer accurately computes the posterior probability of a target (see Figure 2B). The effect of pi node removal is to reduce the both-driven and spontaneous-driven responses to a given input below the values computed by the intact model (see Figures 2B and 2D). Removal of the pi nodes does not eliminate enhancement but reduces it within the enhancement zone (see Figure 2C). These effects are produced over a wide range of model variance and covariance parameters. Binns and Salt (1996) also report that blockade of NMDA receptors in DSC neurons produces reductions in both spontaneous-driven and both-driven responses. For the chosen parameters, the percentage by which the model response is reduced is greater for both-driven than for spontaneous-driven input within the enhancement zone (see Figure 2D), as also observed experimentally. The experimental data are thus more consistent with our hypothesis than with the view that NMDA receptors function as a multiplicative amplifier for CME (see section 5).

4 Multiple Input Channels and Modality-Specific Suppression

The augmented-perceptron model can be extended to account for the fact that cross-modal stimuli produce robust enhancement of DSC neuron re-

sponses, whereas paired modality-specific stimuli do not (Stein & Meredith, 1993). As an implementation of the Bayes' rule model (Anastasio et al., 2000), the augmented perceptron accounts for CME as an increase in the posterior target probability computed by a DSC neuron due to integration of a second input of a different modality. The extension to MSS is based on the intuition that a second input should increase target probability less if it covaries more with the first input and that spontaneous covariance, in particular, is likely to be stronger between inputs of the same modality. Analysis shows this intuition to be correct. Surprisingly, given specific but neurobiologically plausible assumptions concerning the inputs, it can even account for the counterintuitive phenomenon of MSS. Bayes' rule can thus account for both CME and MSS, and both can be implemented using the same augmented perceptron. For convenience, we refer to visual and auditory modalities in what follows, although the result also applies to other modality combinations.

A DSC neuron's visual receptive field is produced by combining input from multiple sources, many of which are known to have much smaller receptive fields than those of DSC neurons (Olson & Graybiel, 1987; Sparks & Hartwich-Young, 1989; Meredith & Stein, 1990). These visual neurons would have separate but overlapping receptive fields within the receptive field of the DSC neuron. We assume that the paired modality-specific stimuli used to produce MSS will activate separate but overlapping sets of visual neurons. We will refer to the set of visual neurons that can be activated by the first stimulus of the pair as channel V and those activated by the second stimulus as channel X. Receptive field overlap will cause the V and X channels to covary under driven conditions. Many of the neurons that provide visual input to the DSC are spontaneously active (see the discussion in Anastasio et al., 2000). Overlap in the sets of visual neurons that comprise channels V and X will cause them to covary under spontaneous conditions. Overlap of spontaneously silent neurons will contribute additional covariance under driven conditions.

In addition to the two visual channels, we assume a third channel A representing auditory input. This three-channel case is treated using an augmented perceptron (see Figure 3A). The means, variances, and covariances for the multivariate gaussians, equation 3.1, representing the spontaneous and driven likelihoods of V, X, and A, are set according to the assumptions made above, which are that means, variances, and covariances are higher under driven than under spontaneous conditions and that covariances, especially spontaneous covariances, are higher between modality-specific than between cross-modal channels. The parameters in the augmented-perceptron model can be computed using equation 3.3 as for the two-channel case above. The model can simulate the finding that cross-modal input pairs (V and A) produce CME, whereas modality-specific input pairs (V and X) do not (see Figures 3B and 3C). To illustrate the explanatory power of the model, the modality-specific case simulated in Figures 3B and 3C is actually one of suppression (MSS).
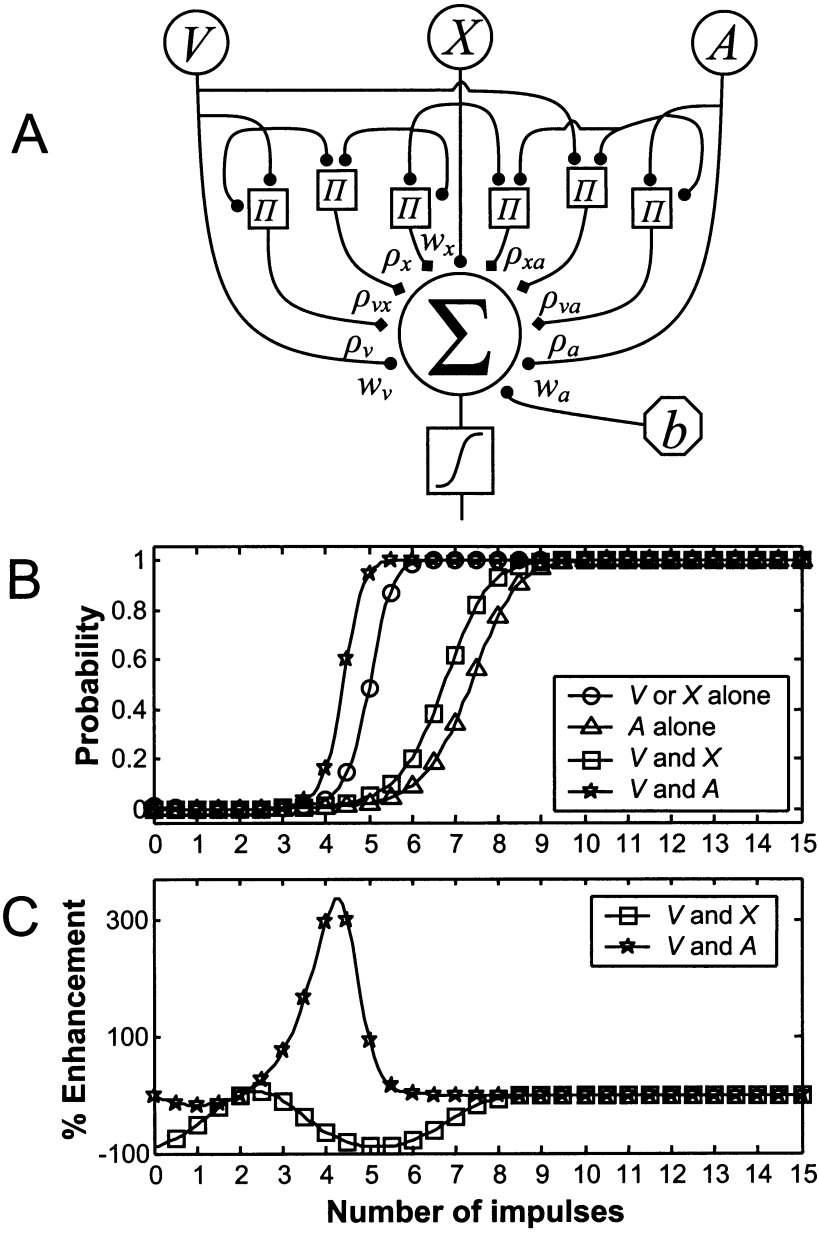
In the model, MSS arises over a specific but neurobiologically plausible range of parameters. Figure 4 shows the effects of varying spontaneous and driven covariance between the V and X channels (σ^2_{vx0} and σ^2_{vx1}) on peak CME and MSS. For the simple case considered, all three modalities have equal spontaneous means ($\mu_{v0} = \mu_{x0} = \mu_{a0} = 2$), driven means ($\mu_{v1} = \mu_{x1} = \mu_{a1} = 6$), spontaneous variances ($\sigma^2_{v0} = \sigma^2_{x0} = \sigma^2_{a0} = 2$), and driven variances ($\sigma^2_{v1} = \sigma^2_{x1} = \sigma^2_{a1} = 6$). Driven covariances between cross-modal channels are larger than spontaneous covariances ($\sigma^2_{va0} = \sigma^2_{xa0} = 0.1, \sigma^2_{va1} = \sigma^2_{xa1} = 2.8$). These parameters are the same as those of Figure 3.

A real-valued multivariate gaussian distribution, equation 3.1, exists only when $|\Sigma_t| > 0$. This condition is met whenever $\sigma^2_v \sigma^2_a \sigma^2_x + 2\sigma^2_{va}\sigma^2_{vx}\sigma^2_{ax} >$

Figure 3: *Facing page*. (A) An augmented-perceptron model of multisensory integration for a three-channel case: $M_1 = V$, $M_2 = X$, and $M_3 = A$. Each channel provides weighted input to summing node Σ with weights w_v, w_x, and w_a. The summing node also receives a fixed bias input b. Each modality multiplies itself and each of the other modalities on the set of six pi nodes Π. The pi nodes provide inputs to the summing node with weights ρ_v, ρ_x, ρ_a, ρ_{vx}, ρ_{xa}, and ρ_{va}. The output of the summing node is passed through the squashing function $f(u)$. (B) A three-channel augmented-perceptron model is used to simulate both CME and MSS. The input likelihoods are multivariate gaussians. The spontaneous input likelihoods for all three channels have means $\mu_{v0} = \mu_{x0} = \mu_{a0} = 2$ and variances $\sigma^2_{v0} = \sigma^2_{x0} = \sigma^2_{a0} = 2$. Driven input likelihoods have means $\mu_{v1} = \mu_{x1} = \mu_{a1} = 6$ and variances $\sigma^2_{v1} = \sigma^2_{x1} = \sigma^2_{a1} = 6$. Within-modality covariances $\sigma^2_{vx0} = 1.6$ and $\sigma^2_{vx1} = 3.6$ are higher than the corresponding between-modality covariances $\sigma^2_{va0} = \sigma^2_{xa0} = 0.1$ and $\sigma^2_{va1} = \sigma^2_{xa1} = 2.8$. The responses are equal to the posterior probability computed by the augmented perceptron. Plots for four different input conditions are shown. For each condition, a driven channel is one where the input varies over the range from 0 to 15 impulses per unit time (abscissa), and a spontaneous channel is one where the input is held fixed at the spontaneous mean. The V or X alone condition (circles) simulates an experiment in which a single visual stimulus is presented. One of the visual channels, V or X, is driven, while the other visual channel and the auditory channel are spontaneous. The A alone case (triangles) simulates an experiment in which an auditory stimulus is presented alone. Channel A is driven, and V and X are spontaneous. The V and X condition (squares) simulates an experiment in which two visual stimuli are presented simultaneously in a DSC neuron's visual receptive field. Channels V and X are driven, and A is spontaneous. The V and A case (stars) simulates an experiment in which a visual and an auditory stimulus are presented simultaneously. Channels V and A are driven, and X is spontaneous. Each plot constitutes a slice through the full 3D posterior. (C) Percentage enhancement is computed as described for Figure 1D. Presentation of two stimuli of different modalities (V and A) produces positive enhancement or CME, while presentation of two stimuli of the same modality (V and X) produces negative enhancement or MSS.

Driven *vx* covariance (σ^2_{vx1})
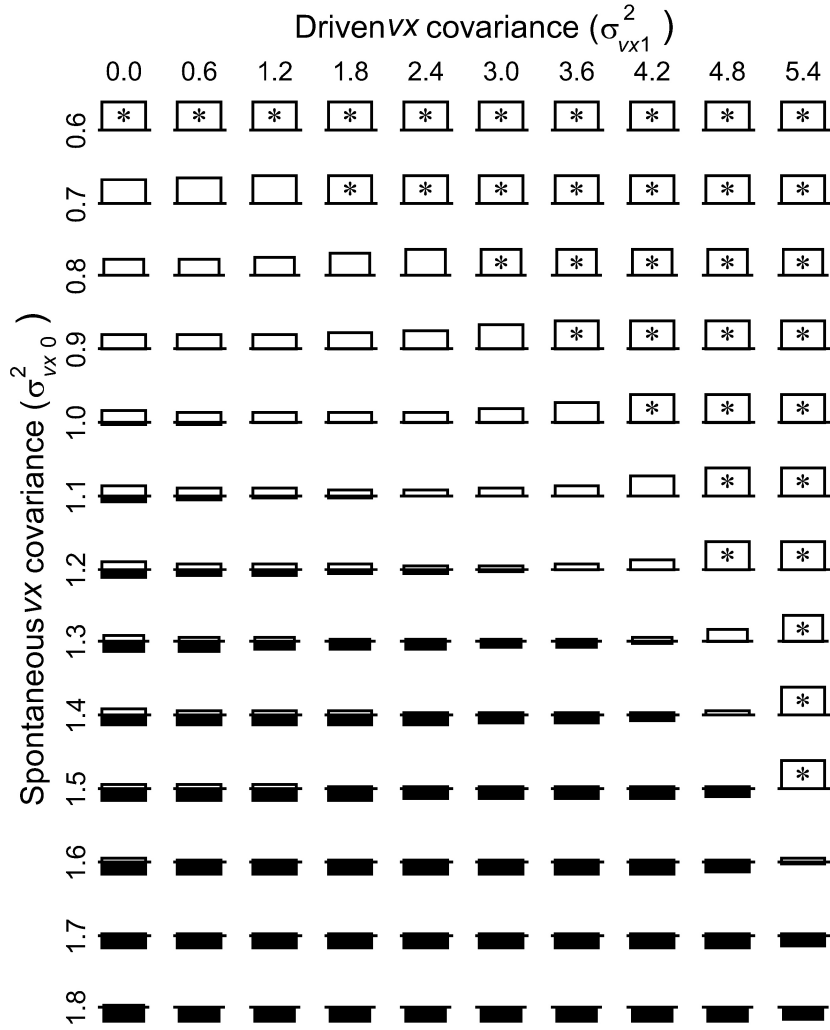
$\sigma^2_v \sigma^4_{ax} + \sigma^2_a \sigma^4_{vx} + \sigma^2_x \sigma^2_{va}$. The chart in Figure 4 is bounded at the right and on the bottom by a region for which no real-valued multivariate gaussian distribution exists. Peak CME (white bars) is always greater than 200% (asterisks) for spontaneous covariance values less than 0.6 (not shown). Suppression (black bars) becomes evident when the spontaneous covariance σ^2_{vx0} approaches the spontaneous variance $\sigma^2_{v0} = \sigma^2_{x0} = \sigma^2_{a0} = 2$, but is relatively uninfluenced by the driven covariance σ^2_{vx1}. Similar relationships are observed when the variances for different modalities are unequal. This

parametric analysis further implicates spontaneous covariance as a factor causing suppression of one input channel by another.

Graphical analysis illustrates how spontaneous covariance between input channels can lead to suppression. It also shows that spontaneous covariance is necessary for suppression but not sufficient, because spontaneous covariance leads to suppression only when driven variance is greater than spontaneous variance. Multivariate gaussian input likelihood distributions ($P(\mathbf{m} \mid T = t)$; see equation 3.1) for the three-channel model are plotted in Figure 5, for a series of different variance and covariance conditions. Figure 6 plots posterior target probabilities ($P(T = 1 \mid \mathbf{m})$; see equation 2.2) for the same series of conditions. The heavy dashed curve in Figure 5 indicates the intersection of the spontaneous and driven likelihood distributions, $P(\mathbf{m} \mid T = 0) = P(\mathbf{m} \mid T = 1)$. For inputs falling on this curve, the posterior probability of a target is equal to its prior probability, $P(T = 1 \mid \mathbf{m}) = P(T = 1)$. The same intersection curve is again shown in Figure 6, which plots posterior target probabilities. In the white region of Figure 6, $P(T = 1 \mid \mathbf{m})$ is nearly 0, and in the gray region nearly 1. In each panel of Figures 5 and 6, the dotted diagonal line indicates the case where channels V and X are held equal and driven over the range from 0 to 15, as in Figure 3. The dot-dashed horizontal line indicates the case where V alone is driven from 0 to 15, and X is held fixed at its spontaneous mean. The dot-dashed vertical line indicates the case where X alone is driven from 0 to 15, with V remaining fixed at its spontaneous mean. In all cases, A channel input is held fixed at its spontaneous mean $\mu_{a0} = 2$.

Figure 4: *Facing page*. Spontaneous covariance is associated with MSS in the three-channel augmented-perceptron model. Spontaneous and driven covariance (σ_{vx0}^2 and σ_{vx1}^2) between the V and X channels are varied, while all other parameters are as specified for Figure 3. Each of the rectangles corresponds to one combination of σ_{vx0}^2 and σ_{vx1}^2, as indicated. VX enhancement was computed by comparing the combined response CR and the maximum single modality response $SR_{\max}$ using equation 1.1. For CR, V and X were both driven by a stimulus over the range from 0 to 30, while A was held fixed at its spontaneous mean. For $SR_{\max}$, V alone was driven over the range from 0 to 30, and X and A were held fixed at their spontaneous means. The maximum percentage enhancement over the range was computed and is indicated for each covariance combination by the height of a white bar above the horizontal line representing zero enhancement. Maximum enhancements exceeding 200% are indicated by a white bar with an asterisk. Spontaneous covariances less than 0.6 (not shown) produced enhancements greater than 200%. The minimum enhancement is computed for inputs that are larger than those at which the maximum occurred. If the minimum observed was less than zero, it is indicated as a black bar extending downward from the horizontal zero enhancement line. The depth of the bar indicates suppression on a scale of 0 to -200%.
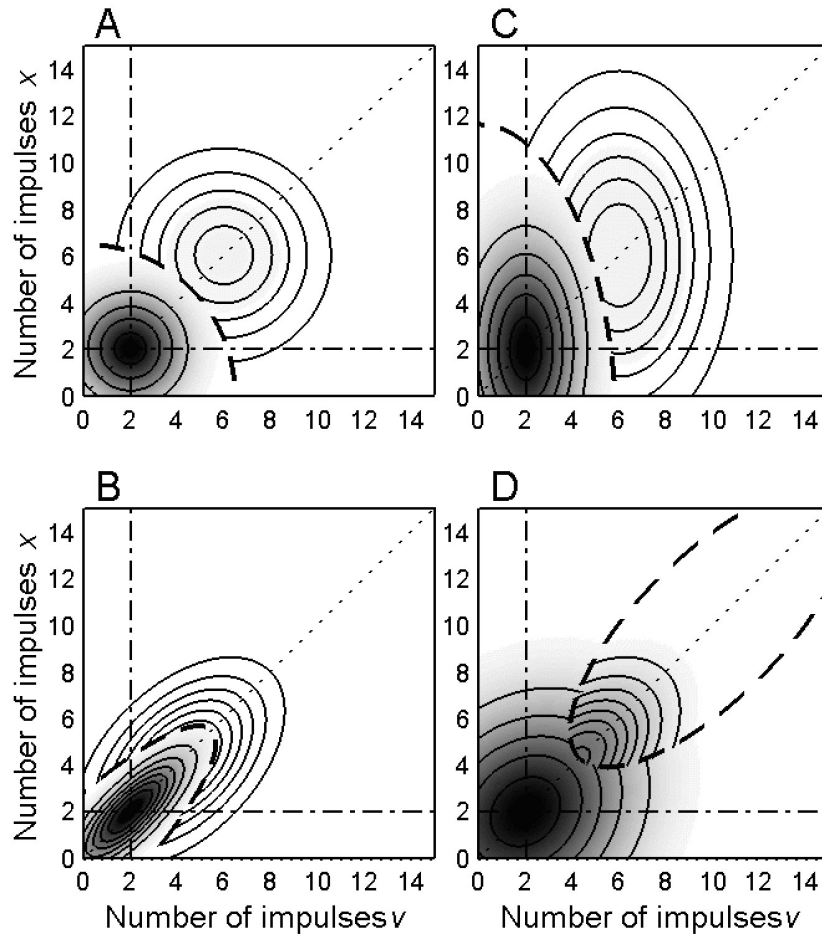
Figure 5: Multivariate gaussian input likelihood distributions for the three-channel model under spontaneous and stimulus-driven conditions for different settings of variance and covariance. In each panel, spontaneous and driven likelihood is plotted as a function of V and X channel input. A channel input is held fixed at its spontaneous mean ($a = \mu_{a0} = 2$). Each plot represents a slice through a 3D likelihood distribution. Likelihood value is indicated by contour lines and shading, where darker shading indicates a higher likelihood. In each panel of Figures 5 and 6, the diagonal dotted line indicates $v = x$, which corresponds to the V- and X-driven case of Figure 3. The horizontal dot-dashed line corresponds to the V-alone case, where v varies from 0 to 15 and $x = a = \mu_{x0} = \mu_{a0} = 2$. The vertical dot-dashed line corresponds to the X-alone case. The heavy dashed curve in each panel indicates the points of intersection of the spontaneous and driven likelihood distributions ($P(\mathbf{m} \mid T = 0) = P(\mathbf{m} \mid T = 1)$). (A) The spontaneous and driven covariances between all channels

Figure 5 (cont.): *Facing page.* are zero ($\sigma^2_{va0} = \sigma^2_{xa0} = \sigma^2_{vx0} = 0, \sigma^2_{va1} = \sigma^2_{xa1} = \sigma^2_{vx1} = 0$). All other parameters are as specified in Figure 3. The concentric contour lines about the point $v = 2$, $x = 2$ indicate the spontaneous likelihood distribution. From outermost to innermost, the contour lines indicate $P(\mathbf{m} \mid T = 0) = 0.005, 0.01, 0.015$, and 0.02, respectively. The concentric contour lines about the point $v = 6$, $x = 6$ indicate the driven likelihood distribution. From outermost to innermost $P(\mathbf{m} \mid T = 1) = 2 \times 10^{-4}, 4 \times 10^{-4}, 6 \times 10^{-4}, 8 \times 10^{-4}$, and 1×10^{-3} respectively. The corresponding posterior target probability distribution is shown in Figure 6A. (B) The spontaneous and driven covariances are nonzero and assigned the same values as for Figure 3 ($\sigma^2_{va0} = \sigma^2_{xa0} = 0.1, \sigma^2_{vx0} = 1.6, \sigma^2_{va1} = \sigma^2_{xa1} = 2.8$, and $\sigma^2_{vx1} = 3.6$). All other parameters are also as specified in Figure 3. The concentric contour lines centered about $v = 2$, $x = 2$ indicate the spontaneous likelihoods $P(\mathbf{m} \mid T = 0) = 0.005, 0.01, 0.015, 0.02, 0.025, 0.03$, and 0.035. The second set of concentric contour lines indicates the driven likelihoods $P(\mathbf{m} \mid T = 1) = 2 \times 10^{-4}, 4 \times 10^{-4}, 6 \times 10^{-4}, 8 \times 10^{-4}, 0.001$, and 0.0012. The corresponding target posterior probability distribution is shown in Figure 6B. (C) The spontaneous and driven covariances between the V, X, and A channels are zero, but the variances are larger for the V channel than for the X and A channels ($\sigma^2_{v0} = 8, \sigma^2_{x0} = \sigma^2_{a0} = 2, \sigma^2_{v1} = 16, \sigma^2_{x1} = \sigma^2_{a1} = 6$). Distribution means are as in Figure 3. The concentric contour lines about $v = 2$, $x = 2$ indicate the spontaneous likelihoods $P(\mathbf{m} \mid T = 0) = 0.002, 0.004, 0.006, 0.008$, and 0.01. The concentric contour lines centered about $v = 6$, $x = 6$ indicate the driven likelihoods $P(\mathbf{m} \mid T = 1) = 1 \times 10^{-4}, 2 \times 10^{-4}, 3 \times 10^{-4}, 4 \times 10^{-4}, 5 \times 10^{-4}$, and 6×10^{-4}. The corresponding target posterior probability distribution is shown in Figure 6C. (D) The spontaneous and driven covariances are nonzero as in Figures 3 and 5B ($\sigma^2_{va0} = \sigma^2_{xa0} = 0.1, \sigma^2_{vx0} = 1.6, \sigma^2_{va1} = \sigma^2_{xa1} = 2.8$, and $\sigma^2_{vx1} = 3.6$), but the spontaneous variance is larger than the driven variance ($\sigma^2_{v0} = \sigma^2_{x0} = \sigma^2_{a0} = 8, \sigma^2_{v1} = \sigma^2_{x1} = \sigma^2_{a1} = 6$). Distribution means are again as for Figure 3. The concentric contour lines about $v = 2$, $x = 2$ indicate the spontaneous likelihoods $P(\mathbf{m} \mid T = 0) = 0.0005, 0.001, 0.0015, 0.002$, and 0.0025. The second set of concentric contour lines indicates the driven likelihoods $P(\mathbf{m} \mid T = 1) = 2 \times 10^{-4}, 4 \times 10^{-4}, 6 \times 10^{-4}, 8 \times 10^{-4}, 0.001, 0.0012, 0.0014$, and 0.0016. The corresponding target posterior probability distribution is shown in Figure 6D.

In Figure 5A the driven variances are equal, the spontaneous variances are equal in all three channels, and driven variance is greater than spontaneous variance, as in Figure 3. Unlike Figure 3, there is no covariance between any of the channels in Figure 5A. Under these circumstances, the spontaneous ($T = 0$) and driven ($T = 1$) likelihood contours (see Figure 5A), and their associated posterior probability contours (see Figure 6A), are circular. The heavy vertical line in Figure 6A connects a point along the V and X both-driven line with the corresponding point along the V-only,
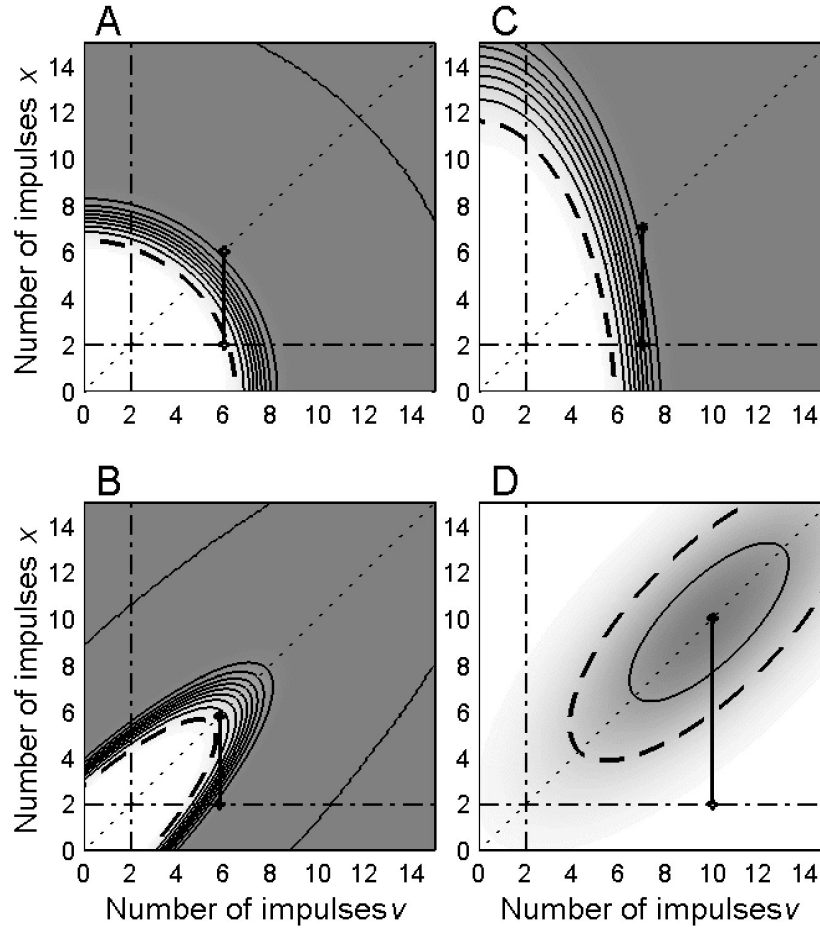
spontaneous-driven line. The both-driven point has posterior probability near one, while the spontaneous-driven point has posterior probability near zero, indicating very large enhancement. For the circular case, Figure 6A illustrates that both-driven posteriors will always be higher than the corresponding spontaneous-driven posteriors and, consequently, suppression cannot occur.

In Figures 5B and 6B, the driven variances are equal, the spontaneous variances are equal again in all three channels, and driven variance is greater than spontaneous variance. Cross-modal channels are assigned a very small spontaneous covariance and a larger driven covariance. The V and X channels are assigned a much larger spontaneous covariance than the cross-modal channels and a larger driven covariance. All parameters have the

same values as for Figure 3. Due to nonzero covariance, the spontaneous and driven likelihood contours (see Figure 5B) are elliptical and elongated in the diagonal direction. The place of intersection of the spontaneous and driven likelihoods, and the posterior probability contours (see Figure 6B), are similarly elliptical and diagonally elongated. This effect is due primarily to the large VX spontaneous covariance. The heavy vertical line in Figure 6B connects a both-driven point having posterior probability near zero with a corresponding spontaneous-driven point having posterior probability near one, indicating suppression. Figure 6B illustrates how suppression can arise from the Bayes' rule model and be simulated by a neural implementation of it when modality-specific channels exhibit spontaneous covariance and driven variance exceeds spontaneous variance.

Figure 6: *Facing page*. Posterior target probability ($P(T = 1 \mid \mathbf{m})$) is plotted as a function of V and X channel input for the three-channel model described in Figure 3. Posterior target probability is indicated in each panel by shading and contour lines. White indicates $P(T = 1 \mid \mathbf{m})$ values near zero, and gray indicates $P(T = 1 \mid \mathbf{m})$ values near one. Contour lines are at 0.1 unit intervals. The heavy dotted curve in each panel indicates the input values for which the posterior and prior target probabilities are equal ($P(T = 1 \mid \mathbf{m}) = P(T = 1) = 0.1$), which is the same as the $P(\mathbf{m} \mid T = 0) = P(\mathbf{m} \mid T = 1)$ curve in the corresponding panels of Figure 5. The dotted and dot-dashed lines are as described in Figure 5. (A) The likelihood parameters are as given for Figure 5A. An input parameter combination that produces enhancement of 1075% is shown by the heavy vertical line terminated with circular dots. The V and X both-driven posterior probability $P(T = 1 \mid V = 6, X = 6, A = 2) = 0.94$ (upper dot) and the V alone posterior $P(T = 1 \mid V = 6, X = 2, A = 2) = 0.08$ (lower dot). (B) The likelihood parameters are as given for Figure 5B. An input parameter combination that produces enhancement of -83.3% (suppression) is shown by the heavy vertical line terminated with circular dots. The V and X both-driven posterior probability $P(T = 1 \mid V = 5.8, X = 5.8, A = 2) = 0.16$ (upper dot) and the V alone posterior $P(T = 1 \mid V = 5.8, X = 2, A = 2) = 0.96$ (lower dot). (C) The likelihood parameters are as given for Figure 5C with different variances for the V and X channels. An input parameter combination that produces enhancement of only 40.3% is shown by the heavy vertical line terminated with circular dots. The V and X both-driven posterior probability $P(T = 1 \mid V = 7, X = 7, A = 2) = 0.94$ (upper dot) and the V alone posterior $P(T = 1 \mid V = 7, X = 2, A = 2) = 0.67$ (lower dot). (D) The likelihood parameters are as described in Figure 5D in which the spontaneous variance is larger than the driven variance. Here, the V and X both-driven posterior probability reaches a maximum value of only 0.27, and thus only two contour lines are visible. An input parameter combination that produces enhancement of 8337% is shown by the heavy vertical line terminated with circular dots. The V and X both-driven posterior probability $P(T = 1 \mid V = 10, X = 10, A = 2) = 0.27$ (upper dot) and the V alone posterior $P(T = 1 \mid V = 10, X = 2, A = 2) = 0.0032$ (lower dot).

Covariance is necessary for suppression. Elongation of the spontaneous or driven likelihoods by itself, without covariance, can decrease enhancement but cannot produce suppression. The spontaneous and driven covariances are set to zero in Figure 5C, but the likelihoods are elongated along the X channel axis (ordinate) by setting the V variance greater than the X variance under both spontaneous and driven conditions. The equal likelihood (see Figure 5C) and posterior probability (see Figure 6C) contours are also elongated along the X channel axis. The heavy vertical line in Figure 6C connects a both-driven point with a corresponding spontaneous-driven point that have almost equal posterior probabilities, indicating very little enhancement. Increasing V variance further would bring the posterior probability contours closer to parallel with the X channel axis. This would further reduce enhancement but never lead to suppression. Suppression requires the elongation combined with diagonalization of likelihood distributions (see Figures 5B and 6B) that can be produced only by covariance.

Covariance is necessary but not sufficient for suppression. Suppression requires spontaneous covariance (with or without driven covariance), and that driven variance is greater than spontaneous variance. In Figures 5D and 6D, channel covariances are as in Figures 5B and 6B, and the spontaneous variances are equal and the driven variances are equal for all three channels. Unlike the case of Figures 5B and 6B, the driven variance in Figures 5D and 6D is smaller than the spontaneous variance. Now the heavy dashed curve indicating equal spontaneous and driven likelihood (see Figure 5D) and equal prior and posterior probability (see Figure 6D) forms a closed ellipse containing the point specified by the driven V and X means. The spontaneous-driven lines never intersect this ellipse. Within the ellipse, the posterior probability of a target never exceeds 0.27. The heavy vertical line in Figure 6D connects a both-driven point having posterior probability 0.27 with a spontaneous-driven point having posterior probability near zero, producing sizable enhancement only because of the small magnitude of the latter value.

In summary, suppression can occur between two channels when driven variance is larger than spontaneous variance and spontaneous covariance approaches the value of spontaneous variance (with or without driven covariance). These conditions are very likely to be met by channels of the same modality that provide input to neurons in the DSC and elsewhere in the brain (see above). It is very likely that driven variance will be higher than spontaneous variance, because driven variance reflects the huge variability in stimulus effectiveness, in addition to the stochastic properties of the nervous system that determine spontaneous variance. It is also very likely that input channels of the same modality will covary under both spontaneous and driven conditions, because they may share some of the same input axons. The seemingly paradoxical phenomenon of MSS arises naturally from the Bayes' rule model of CME, given these neurobiologically plausible conditions of input channel variance and covariance. The three-channel neural

implementation presented in Figure 3 illustrates an example in which CME and MSS can arise in the same model neuron. The implementation can be extended to any number of cross-modal and modality-specific channels. A two-channel, single-modality model was also investigated, and suppression was found to occur under similar parametric circumstances.

5 Discussion

CME is often referred to as supra-additive or multiplicative, since a neuron's response to multimodal stimuli is often greater than the sum of the responses to the single modality stimuli presented alone (Meredith & Stein, 1986b; Stein et al., 1988; Meredith et al., 1992; Stein & Meredith, 1993). It has been suggested that CME requires a special nonlinear amplifier, such as an ion channel, that responds to multimodal but not unimodal input (Stein & Meredith, 1993; Binns & Salt, 1996; Binns, 1999). The implementations we have examined here suggest a different view of cross-modal enhancement.

We have previously argued that CME arises as a consequence of DSC neurons computing the posterior probability of a target using Bayes' rule (Anastasio et al., 2000). Here we use neural implementations of the Bayes' rule model to address issues of neurobiological mechanism. A single perceptron is capable of computing the target posterior when the inputs are conditionally independent and Poisson distributed, or gaussian distributed without the assumption of conditional independence, provided variances and covariances for the spontaneous likelihood distribution are equal to those for the driven likelihood distribution. When the above equality is not satisfied, an augmented perceptron, which allows inputs to be multiplied together, is needed to compute the posterior probability of a target. In either case, CME itself is produced by weighted summation in a nonlinear model neuron. Multiplication of inputs is not needed to produce CME. Instead, it serves a function not envisioned by the multiplicative amplifier hypothesis. It serves to compensate for differences between spontaneous and driven variance and covariance, to allow computation of posterior target probability when these parameters are unequal.

It has been suggested that NMDA-sensitive glutamate conductances present in DSC neurons might provide a multiplicative amplifier for CME (Stein & Meredith, 1993; Binns & Salt, 1996; Binns, 1999). Binns and Salt (1996) tested this hypothesis by applying the NMDA receptor antagonist AP5 to multisensory DSC neurons in the cat during cross-modal and modality-specific stimulation. The results were equivocal with respect to the amplifier hypothesis, since AP5 did not selectively eliminate CME. Instead, application of AP5 resulted in a reduction of both modality-specific and cross-modal responses, with the percentage reduction being greater for the latter. It is possible to reconcile these findings with the multiplicative hypothesis by proposing, for example, that NMDA receptors involved in cross-modal responses have different channel kinetics from those involved in modality-

specific responses (Binns, 1999). Our model, however, can account for the findings without any such special assumptions.

The function of the pi nodes in the augmented perceptron model might be implemented by dendritic voltage-sensitive conductances in DSC neurons (Koch & Poggio, 1992; Mel, 1993). We propose that rather than serving as multiplicative amplifiers for CME, NMDA receptors in DSC neurons might perform the function of these pi nodes. Simulations in which pi nodes were removed from the model, over a suitable range of parameters, yielded results similar to those observed in the NMDA channel blockade studies. Removing the pi nodes from the augmented-perceptron model similarly produced a reduction in response to both modality-specific and cross-modal stimuli, with the percentage reduction being greater for the latter (see Figure 2C). Our model provides a straightforward explanation for the NMDA channel blockade findings, whereas the amplifier model of CME does not.

In addition to multimodal interactions, Stein and Meredith (1993) have examined interactions between two stimuli of the same modality. Given the assumptions that driven variances are greater than the spontaneous variances and that significant spontaneous covariance should occur between modality-specific but not between cross-modal input channels, the augmented-perceptron implementation simulated the absence of enhancement for modality-specific stimuli and the presence of enhancement for cross-modal stimuli. Furthermore, our model proved capable of simulating the counterintuitive finding of modality-specific suppression. For suppression to occur in the model, the spontaneous covariance between the V and X channels must be less than, but close to, the spontaneous variances. When these conditions are met, the VX pi node invariably has a negative weight ($\rho_{vx} < 0$). Neurobiologically, a pi node with a negative weight might correspond, for example, to an inhibitory interneuron with a nonlinear conductance perhaps produced by NMDA receptors.

Depressive interactions, in which the neural response to a cross-modal stimulus is less than that elicited by a single stimulus, can occur when the two stimuli are sufficiently spatially disparate (Meredith & Stein, 1986a, 1986b, 1996; Kadunce, Vaughan, Wallace, Benedek, & Stein, 1997; Kadunce et al., 2001). Pairs of modality-specific stimuli can also produce such effects when one of the two is outside the excitatory receptive field (Kadunce et al., 1997). This is distinct from the modality-specific suppression discussed above, in which both stimuli are presented within the excitatory receptive field. Depression due to spatial disparity appears to result from competitive interactions involved in target selection (Munoz & Istvan, 1998; Findlay & Walker, 1999) rather than target detection, which is the focus of this study. Our results do not preclude competitive interaction as a possible explanation for modality-specific suppression. They do demonstrate that modality-specific suppression can be simulated using the Bayes' rule model of CME and neural implementations thereof and is therefore a plausible consequence of target detection processes.

CME in the DSC apparently depends on cortical-descending input. The DSC of the cat receives descending cortical input from certain areas of extraprimary sensory cortex, including the anterior ectosylvian cortex (AES) and the lateral suprasylvian sulcus (Berson & McIlwain, 1983; Harting, Updyke, & Van Lieshout, 1992; Wallace et al., 1993). Inactivation of these areas, and of AES in particular, has been shown to selectively abolish CME, while preserving multisensory responsiveness in DSC neurons (Wallace & Stein, 1994; Jiang, Wallace, Jiang, Vaughan, & Stein, 2001). The model suggests that the cortical input could produce CME simply by adding a component to the DSC response to subcortical input, but it offers no insight into how the cortical and subcortical contributions may be partitioned. We are exploring a new model that subsumes the implementations proposed here within a broader model of the development of CME, using intrinsic Hebbian mechanisms and both ascending and cortical-descending inputs to the DSC.

For the case of conditionally independent Poisson distributed inputs, the bias b is negative whenever $P(T = 1) < P(T = 0)$ and $\lambda_{i0} < \lambda_{i1}$. For the more general case, the value of b is influenced by all of the other parameters in the model (see equation 3.9). A number of restricted cases were examined, and it was found that b was negative for all but a small portion of parameter space (near asymptotes) whenever a set of plausible parameter requirements was maintained. The inhibitory bias might correspond to some biophysical mechanism intrinsic to DSC neurons or to an extrinsic source of tonic inhibition. The DSC contains inhibitory interneurons and receives extrinsic inhibitory input from the substantia nigra, zona incerta, contralateral colliculus, and a variety of brainstem structures (Karabelas & Moschovakis, 1985; Ficalora & Mize, 1989; Appell & Behan, 1990; Mize, 1992; May, Sun, & Hall, 1997). Both substantia nigra and zona incerta cells are tonically active (Hikosaka & Wurtz, 1983; Ma, 1996). Some substantia nigra cells respond to visual or auditory stimulation with a decrease or cessation of firing. Because the bias contains a term related to the target prior probability, it is possible that the sensory responses of nigral cells could modulate CME in the DSC according to changes in the prior expectation of targets.

References

Anastasio, T. J., Patton, P. E., & Belkacem-Boussaid, K. (2000). Using Bayes' rule to model multisensory enhancement in the superior colliculus. *Neural Computation, 12*, 997–1019.

Appell, P. P., & Behan, M. (1990). Sources of subcortical GABAergic projections to the superior colliculus in the cat. *J. Comp. Neurol., 302*(1), 143–158.

Berson, D. M., & McIlwain, J. T. (1983). Visual cortical inputs to the deep layers of cat's superior colliculus. *J. Neurophysiol., 50*, 1143–1155.

Binns, K. E. (1999). The synaptic pharmacology underlying sensory processing in the superior colliculus. *Prog. Neurobiol., 59*(2), 129–159.

Binns, K. E., & Salt, T. E. (1996). Importance of NMDA receptors for multimodal integration in the deep layers of the cat superior colliculus. *J. Neurophysiol., 75*(2), 920–930.

Clemo, H. R., & Stein, B. E. (1991). Receptive field properties of somatosensory neurons in the cat superior colliculus. *J. Comp. Neurol., 314*(3), 534–544.

Cybenko, G. (1989). Approximation by superpositions of a sigmoidal function. *Mathematics of Control, Signals, and Systems, 2*, 303–314.

Duda, R. O., Hart, P. E., & Stork, D. G. (2001). *Pattern classification* (2nd ed.). New York: Wiley.

Durbin, R., & Rumelhart, D. E. (1989). Product units: A computationally powerful and biologically plausible extension to backpropagation networks. *Neural Computation, 1*, 133–142.

Ficalora, A. S., & Mize, R. R. (1989). The neurons of the substantia nigra and zona incerta which project to the cat superior colliculus are GABA immunoreactive: A double label study using GABA immunocytochemistry and lectin retrograde transport. *Neurosci., 29*, 567–581.

Findlay, J. M., & Walker, R. (1999). A model of saccade generation based on parallel processing and competitive inhibition. *Behav. Brain Sci., 22*, 661–721.

Fristedt, B., & Gray, L. (1997). *A modern approach to probability theory*. Boston: Birkhäuser.

Gabbiani, F., & Koch, C. (1998). Principles of spike train analysis. In C. Koch & I. Segev (Eds.), *Methods in neuronal modeling* (2nd ed., pp. 312–360). Cambridge, MA: MIT Press.

Harting, J. K., Updyke, B. V., & Van Lieshout, D. P. (1992). Corticotectal projections in the cat: Anterograde transport studies of twenty-five cortical areas. *J. Comp. Neurol., 324*(3), 379–414.

Hikosaka, O., & Wurtz, R. H. (1983). Visual and oculomotor functions of the monkey substantia nigra pars reticulata. I. Relation of visual and auditory responses to saccades. *J. Neurophysiol., 49*, 1254–1267.

Jiang, H., Lepore, F., Ptito, M., & Guillemot, J.-P. (1994). Sensory interactions in the anterior ectosylvian cortex of cats. *Exp. Brain Res., 101*, 385–396.

Jiang, W., Wallace, M. T., Jiang, H., Vaughan, J. W., & Stein, B. E. (2001). Two cortical areas mediate multisensory integration in superior colliculus neurons. *J. Neurophysiol., 85*, 506–522.

Kadunce, D. C., Vaughan, J. W., Wallace, M. T., Benedek, G., & Stein, B. E. (1997). Mechanisms of within- and cross-modality suppression in the superior colliculus. *J. Neurophysiol., 78*(6), 2834–2847.

Kadunce, D. C., Vaughan, J. W., Wallace, M. T., & Stein, B. E. (2001). The influence of visual and auditory receptive field organization on multisensory integration in the superior colliculus. *Exp. Brain Res., 139*, 303–310.

Karabelas, A. B., & Moschovakis, A. K. (1985). Nigral inhibitory termination on efferent neurons of the superior colliculus: An intracellular horseradish peroxidase study in the cat. *J. Comp. Neurol., 239*(3), 309–329.

Koch, C., & Poggio, T. (1992). Multiplying with synapses and neurons. In T. McKenna, J. L. Davis, & S. F. Zornetzer (Eds.), *Single neuron computation* (pp. 315–345). San Diego, CA: Academic Press.

Ma, T. P. (1996). Saccade related omnivectorial pause neurons in the primate zona incerta. *NeuroReport, 7*, 2713–2716.

May, P. J., Sun, W., & Hall, W. C. (1997). Reciprocal connections between the zona incerta and the pretectum and superior colliculus of the cat. *Neurosci., 77*(4), 1091–1114.

Mel, B. W. (1993). Synaptic integration in an excitable dendritic tree. *J. Neurophysiol., 70*(3), 1086–1101.

Meredith, M. A., & Stein, B. E. (1986a). Spatial factors determine the activity of multisensory neurons in cat superior colliculus. *Brain Res., 365*(2), 350–354.

Meredith, M. A., & Stein, B. E. (1986b). Visual, auditory, and somatosensory convergence on cells in superior colliculus results in multisensory integration. *J. Neurophysiol., 56*(3), 640–662.

Meredith, M. A., & Stein, B. E. (1990). The visuotopic component of the multisensory map in the deep laminae of the cat superior colliculus. *J. Neurosci., 10*(11), 3727–3742.

Meredith, M. A., & Stein, B. E. (1996). Spatial determinants of multisensory integration in cat superior colliculus neurons. *J. Neurophysiol., 75*(5), 1843–1857.

Meredith, M. A., Wallace, M. T., & Stein, B. E. (1992). Visual, auditory and somatosensory convergence in output neurons of the cat superior colliculus: Multisensory properties of the tecto-reticulo-spinal projection. *Exp. Brain Res., 88*(1), 181–186.

Middlebrooks, J. C., & Knudsen, E. I. (1984). A neural code for auditory space in the cat's superior colliculus. *J. Neurosci., 4*(10), 2621–2634.

Mize, R. R. (1992). The organization of GABAergic neurons in the mammalian superior colliculus. *Prog. Brain Res., 90*, 219–248.

Munoz, D. P., & Istvan, P. J. (1998). Lateral inhibitory interactions in the intermediate layers of the monkey superior colliculus. *J. Neurophysiol., 79*(3), 1193–1209.

Olson, C. R., & Graybiel, A. M. (1987). Ectosylvian visual area of the cat: Location retinotopic organization, and connections. *J. Comp. Neurol., 261*, 277–294.

Peck, C. K. (1990). Neuronal activity related to head and eye movements in cat superior colliculus. *J. Physiol. (Lond.), 421*, 79–104.

Reynolds, J. H., Chelazzi, L., & Desimone, R. (1999). Competitive mechanisms subserve attention in macaque areas V2 and V4. *Journal of Neuroscience, 19*(5), 1736–1753.

Richard, M. D., & Lippmann, R. P. (1991). Neural network classifiers estimate Bayesian a posteriori probabilities. *Neural Computation, 3*, 461–483.

Rumelhart, D. E., Hinton, G. E., & McClelland, J. L. (1986). A general framework for parallel distributed processing. In D. E. Rumelhart & J. L. McClelland (Eds.), *Parallel distributed processing: Explorations in the microstructure of cognition* (Vol. 1, pp. 45–76). Cambridge, MA: MIT Press.

Sato, T. (1989). Interactions of visual stimuli in the receptive fields of inferior temporal neurons in awake macaques. *Exp. Brain Res., 77*, 23–30.

Sato, T. (1995). Interactions between two different visual stimuli in the receptive fields of inferior temporal neurons in macaques during matching behaviors. *Exp. Brain Res., 105*, 209–219.

Sparks, D. L., & Hartwich-Young, R. (1989). The deep layers of the superior colliculus. In R. H. Wurtz & M. Goldberg (Eds.), *The neurobiology of saccadic eye movements* (Vol. 3, pp. 213–255). Amsterdam: Elsevier.

Stein, B. E., Huneycutt, W. S., & Meredith, M. A. (1988). Neurons and behavior: The same rules of multisensory integration apply. *Brain Res., 448*(2), 355–358.

Stein, B. E., & Meredith, M. A. (1993). *The merging of the senses*. Cambridge, MA: MIT Press.

Stein, B. E., Meredith, M. A., Huneycutt, W. S., & McDade, L. (1989). Behavioral indices of multisensory integration: Orientation to visual cues is affected by auditory stimuli. *J. Cog. Neurosci., 1*(1), 12–24.

Stein, B. E., & Wallace, M. T. (1996). Comparisons of cross-modality integration in midbrain and cortex. *Prog. Brain Res., 112*, 289–299.

Wallace, M. T., Meredith, M. A., & Stein, B. E. (1992). Integration of multiple sensory modalities in cat cortex. *Exp. Brain Res., 91*(3), 484–488.

Wallace, M. T., Meredith, M. A., & Stein, B. E. (1993). Converging influences from visual, auditory, and somatosensory cortices onto output neurons of the superior colliculus. *J. Neurophysiol., 69*(6), 1797–1809.

Wallace, M. T., Meredith, M. A., & Stein, B. E. (1998). Multisensory integration in the superior colliculus of the alert cat. *J. Neurophysiol., 20*(2), 1006–1010.

Wallace, M. T., & Stein, B. E. (1994). Cross-modal synthesis in the midbrain depends on input from cortex. *J. Neurophysiol., 71*(1), 429–432.

Wallace, M. T., Wilkinson, L. K., & Stein, B. E. (1996). Representation and integration of multiple sensory inputs in primate superior colliculus. *J. Neurophysiol., 76*(2), 1246–1266.

Wurtz, R. H., & Goldberg, M. E. (1972). Activity of superior colliculus in behaving monkey. III. Cells discharging before eye movements. *J. Neurophysiol., 35*(4), 575–586.